

Quantum elliptic vortex in a nematic-spin Bose-Einstein condensate

Hiromitsu Takeuchi*

Department of Physics and Nambu Yoichiro Institute of Theoretical and Experimental Physics (NITEP),
Osaka City University, Osaka 558-8585, Japan

(Dated: December 22, 2024)

A novel vortex in a spin-nematic superfluid is found theoretically. A vortex spontaneously breaks its axisymmetry, leading to an elliptic vortex in nematic-spin Bose-Einstein condensates with small positive quadratic Zeeman effect. The new vortex is considered the Joukowski transform of a conventional quantized vortex. Its oblateness grows when the Zeeman length scale exceeds the spin healing length. This structure is sustained by balancing the hydrodynamic potential and the elasticity of a soliton connecting two magnetized spots, which is experimentally observed by *in situ* magnetization imaging.

Unconventional superfluids, such as spin-triplet p -wave superfluid ^3He and binary/spinor Bose-Einstein condensates (BECs) [1–3], exhibit properties similar to uniaxial nematic liquid crystals (NLCs) [4]. In such superfluids called the nematic-spin superfluids [5–7], the order parameter is partly represented by a vector $\hat{\mathbf{d}}$ that mimics the *director* $\hat{\mathbf{d}}$ in the NLC. Nematic-spin superfluids support not only conventional topological defects in NLC (disclination, hedgehog, domain wall, and boojum [8–18]), but also novel defects combined with the superfluidity. An important example is a quantum counterpart of a half disclination, called the half quantum vortex (HQV) [19]. The simplest type of HQV has been realized experimentally in different superfluids [20–22], where the core of the vortex in one (spin) component is occupied by the other vortex-free component. A nontrivial type of HQV is terminated by a domain wall across which the order parameter has a phase difference π . This is called the wall-HQV composite.

Wall-HQV composites were first realized as the double-core vortices in superfluid ^3He by the Helsinki group [23]. The research interest in wall-HQVs has been revived recently [24–26], motivated by a cosmological scenario in which the composites of the Kibble-Lazarides-Shafi (KLS) walls and vortex strings are nucleated via phase transitions in the early universe [27–29]. The Seoul group has observed wall-HQV composites nucleated via quenched phase transition from the antiferromagnetic (AF) phase to the polar (P) phase in a spinor BEC of ^{23}Na atoms [30, 31]. The experiments [30, 31] are groundbreaking by observing the non-equilibrium dynamics of wall-HQV composites directly. However, the phase ordering dynamics are poorly understood, because of the lack of precise knowledge about the properties of wall-HQV composites. Determining these properties is important, because they are fundamental to double-core vortex in superfluid $^3\text{He-B}$ [32–36] and Berezinskii-Kosterlitz-Thouless transition in anti-ferromagnetic BECs [37–39].

In this study, a free wall-HQV composite in the P phase of spin-1 BECs has been investigated theoretically. It is shown numerically that a quantized vortex forms a non-axisymmetric structure called the elliptic vortex in

the critical regime of the small positive quadratic Zeeman effect (Fig. 1). The elliptic vortex is interpreted as the equilibrium state of the free wall-HQV composite [30, 31], and exhibits an exotic hydrodynamic property. It forms a planar singularity with elliptic velocity fields, regarded as the Joukowski mapping of a point vortex. Elliptic vortices have different scaling behaviors based on three length scales associated with the Zeeman effect, the spin interaction, and the condensation energy [Fig. 2]. It is detectable in the presence of a macroscopic magnetic structure [Figs. 1(b,c) and 3(b)].

Formulation— A spin-1 BEC of ^{23}Na atoms is described by the condensate wave function Φ_m ($m = 0, \pm 1$) of the $|m\rangle$ Zeeman component in the Gross-Pitaevskii (GP) model at zero temperature [3, 40]. The thermodynamic energy is represented as $G(\{\Phi_m\}) = \int d^3x \mathcal{G}$, with $\mathcal{G} = \frac{\hbar^2}{2M} \sum_m |\nabla \Phi_m|^2 + \mathcal{U}$, and

$$\mathcal{U} = \frac{c_0}{2} n^2 + \frac{c_2}{2} \mathbf{s}^2 - (\mu - q)n - q |\Phi_0|^2 - p s_z. \quad (1)$$

Here, we introduced the chemical potential $\mu (> 0)$ and the coefficient q (p) of the quadratic (linear) Zeeman effect. In the Cartesian representation $\Phi = [\Phi_x, \Phi_y, \Phi_z]^T = \left[\frac{-i}{\sqrt{2}}(\Phi_{+1} - \Phi_{-1}), \frac{i}{\sqrt{2}}(\Phi_{+1} + \Phi_{-1}), \Phi_0 \right]^T$ [41], the condensate density and the spin density are expressed by the dot product $n = \sum_m |\Phi_m|^2 = \Phi^* \cdot \Phi$, and the cross product $\mathbf{s} = [s_x, s_y, s_z]^T = i \Phi \times \Phi^*$, respectively.

The ground (bulk) state is obtained by minimizing the condensation energy $U = \int d^3x \mathcal{U}$. Assuming the antiferromagnetic interaction $c_2 = 0.016c_0 > 0$ with $p = 0$ obtained experimentally [30, 31], the ground state has no magnetization ($\mathbf{s} = 0$), and the order parameter is represented as

$$\Phi = \sqrt{n} e^{i\theta_G} \hat{\mathbf{d}}. \quad (2)$$

The real unit vector $\hat{\mathbf{d}} = [d_x, d_y, d_z]^T$ plays the role of *pseudo-director*; an ordered state of $(\hat{\mathbf{d}}, \theta_G)$ is identical to that of $(-\hat{\mathbf{d}}, \theta_G + \pi)$. The ground state in the P (AF) phase with $q > 0$ ($q < 0$) is represented as $n = n_P$ and $\hat{\mathbf{d}} = \pm \hat{\mathbf{z}}$ ($n = n_{AF}$ and $\hat{\mathbf{d}} = \hat{\mathbf{r}}_{\perp}$), where the bulk

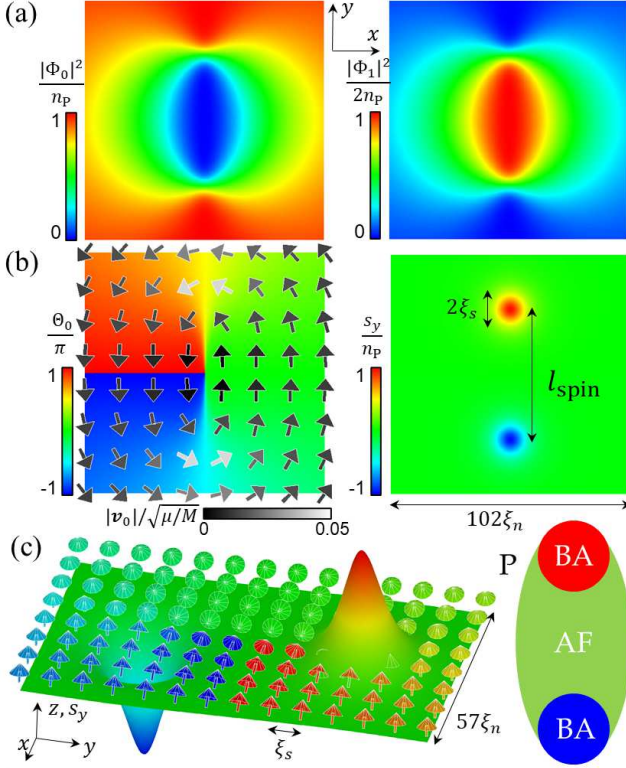


FIG. 1. The cross-sectional profile of an elliptic vortex for $q/\mu = 2^{-17} \approx 7.6 \times 10^{-6}$. (a) The left and right panels show the density profiles of $\frac{|\Phi_0|^2}{n_P}$ and $\frac{|\Phi_1|^2}{2n_P}$, respectively. The profile of $|\Phi_{-1}|^2$ is not shown, since it is the same as that of $|\Phi_1|^2$. (b) The vector field on the left shows $\mathbf{v}_0 = \frac{\hbar}{M} \nabla \Theta_0$, with the background plot of $\Theta_0 = \arg \Phi_0$. The phase arg $\Phi_{\pm 1}$ is homogeneous in the core (not shown). The spin density s_y is plotted on the right, while $s_x = s_z = 0$. (c) (Left) The texture of the unit vector $\mathbf{d}/|\mathbf{d}|$ (arrow) in Eq. (2). The color of the arrows and the surface correspond to Φ_0 and s_y in (b), respectively. (Right) A schematic of the cross-sectional profile.

density is given by $n_P = \frac{\mu}{c_0}$ ($n_{AF} = \frac{\mu - q}{c_0}$), and the unit vector $\hat{\mathbf{z}}$ ($\hat{\mathbf{r}}_{\perp}$) parallel (normal) to the spin quantization axis. By rescaling energy and length by μ and $\xi_n \equiv \frac{\hbar}{\sqrt{M\mu}}$, respectively, the P phase is parameterized by two dimensionless quantities, $\frac{c_2}{c_0}$ and $\frac{q}{\mu}$.

Vortex core structure— One might expect that there is nothing strange about the occurrence of vortices in P phase, where the order parameter is a complex scalar $\Phi_0 = \sqrt{n_P} e^{i\Theta_0}$ with $\Phi_{\pm 1} = 0$, as is in conventional scalar superfluids. However, the vortex core can be unconventional. This behavior is typical in nematic-spin superfluids; The core of the topological defects is occupied by a different ordered state so as to reduce the condensation energy. Similarly, the core of a vortex in the P phase can be occupied by the $m = \pm 1$ component.

To examine the conjecture, the lowest-energy solution was obtained in a uniform system numerically. It is found

that a non-axisymmetric core structure is observed for small q/μ . Figure 2 shows the cross-section of the non-axisymmetric core, obtained numerically by minimizing the energy G in a uniform system [42, 43]. The vortex core of the $m = 0$ component is occupied by the $m = \pm 1$ components, and the density n is mostly homogeneous [Fig. 1(a)]. Surprisingly, the velocity field forms an elliptic structure [Fig. 1(b) left]. Additionally, two spin spots are observed with opposite transverse magnetization ($s_y \neq 0$) at the edges of the vortex core [Fig. 1(b) right].

The distance l_{spin} between the two spin spots is a decreasing function of q [Fig. 2(a)]. Accordingly, the density n_{core} at the center of the vortex core and the maximum spin density s_{\perp}^{max} decrease with q and vanish at a critical value $q_C \approx 0.25\mu$ [Fig. 2(b)] [44, 45]. This behavior is partly similar to that of the AF-core soliton in polar phase [46], where the soliton core is vacant for large q , while the core is occupied by the AF state ($\mathbf{s} = 0$ with $\Phi_{\pm 1} \neq 0$ and $\Phi_0 \approx 0$) below q_C . In our case, however, the vortex core is occupied by two different states, the Broken-axisymmetry (BA) state ($\mathbf{s} \perp \hat{\mathbf{z}}$ with $\Phi_1 \Phi_0 \Phi_{-1} \neq 0$) [47], in addition to the AF state.

To explain the core structure of an elliptic vortex schematically, it is useful to introduce the representation

$$\Phi = e^{i\Theta_0} (\mathbf{d} + i\mathbf{e}_{\perp}) \quad (3)$$

with the real vectors $\mathbf{d} = [d_x, d_y, d_z]^T$ with $d_z \geq 0$, and $\mathbf{e}_{\perp} \perp \hat{\mathbf{z}}$. Equation (3) reduces Eq. (2) for $\mathbf{s} = 0$, with $\mathbf{e}_{\perp} = 0$ and $\mathbf{d} = \sqrt{n} \hat{\mathbf{d}}$ [48]. The left panel in Fig 1(c) shows a cross-sectional plot of $\frac{\mathbf{d}}{|\mathbf{d}|}$ and s_y . In the center region between the two spin spots, \mathbf{d} lies on the xy -plane forming the AF state, where a state $(\hat{\mathbf{d}}, \theta_G) = (-\hat{\mathbf{x}}, \pm\pi)$ for $x > 0$ is identical to $(\hat{\mathbf{x}}, 0)$ for $x < 0$ along the center line $x = 0$. The nematic-spin order is destroyed when $\hat{\mathbf{d}}$ is ill-defined in the spin spot occupied by the BA state, as described schematically on the right panel in Fig 1(c).

To clarify our problem, the main goal is to answer the following two questions;

Q1: What causes the axisymmetry breaking?

Q2: What is the physical mechanism to stabilize the elliptic structure?

Vortex winding rule— As the answer for the first question, it is claimed that the spin interaction breaks the axisymmetry. To justify the claim logically, we introduce a winding rule of an axisymmetric vortex in spin-1 BECs. We consider a straight vortex along the z axis, the cross section of which is axisymmetric as $\Phi_m = f_m(r) e^{iL_m\varphi}$, with radius $r = \sqrt{x^2 + y^2}$, and azimuthal angle φ in cylindrical coordinates. The rule states that L_m is parameterized by the winding numbers L and N , associated with the mass- and spin-current, respectively, and given by

$$L_m = L + mN \quad (L, N = 0, \pm 1, \pm 2, \dots) \quad (4)$$

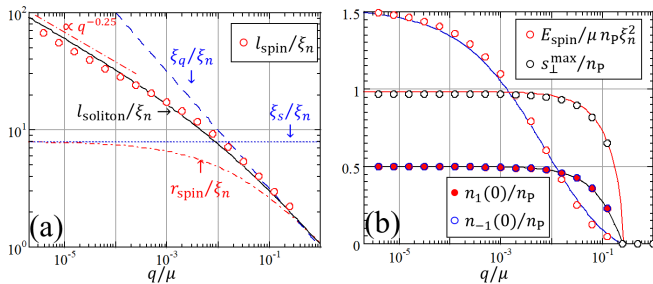


FIG. 2. (a) The q -dependence of l_{spin} . The solid curve represents the evaluation by Eq. (12). All lengths are scaled by ξ_n . (b) The q -dependence of the spin interaction E_{spin} , the maximum spin density $s_{\perp}^{\text{max}} = \max(s_y)$, and the core density $n_{\pm 1}(0)$. The solid curve tracing each data corresponds to an analytic formula (see text).

This rule is applicable only when the real functions $f_m(r)$ ($m = 0, \pm 1$) are nonzero [49, 50].

By contraposition of the above argument, the vortex must be non-axisymmetric, when the winding rule is not satisfied. As is seen in Fig. 1, only the $m = 0$ component has a nonzero winding number, corresponding to $L_0 = 1$ and $L_{\pm 1} = 0$. Such a set of winding numbers cannot satisfy the winding rule. The axisymmetry is exactly recovered only for $\Phi_{\pm 1} = 0$ ($q \geq q_c$).

The spin interaction is essential to the axisymmetry breaking. The energy terms other than the spin interaction in the energy functional G have a quadratic dependence on the order parameter given by $|\Phi_m|^2 \rightarrow f_m^2$. The winding rule is directly connected with the transverse component of the spin density, depending on $\arg \Phi_m$ [51]. This is the reason why the spin spots exhibit transverse magnetization.

Joukowski mapping— To answer the second question, the potential flow theory in two-dimensional flow is extended to our problem. The elliptic core structure hints at the Joukowski transformation, since the velocity field on the cross-section is considered a two-dimensional potential flow [52–54]. This perception is the motivation for investigating the problem, and the following analysis lead to the evaluation of the elliptic core structure quantitatively.

The velocity field $\mathbf{v}_0 = \frac{\hbar}{M} \nabla \Theta_0 = (u, v)$ in the xy -plane is generated by a conformal mapping called the Joukowski transformation from a vortex within a cylinder of radius a in the ζ complex plane to the xy -plane, $x + iy = \zeta + \frac{a^2}{\zeta}$. By using the parameterization $\zeta = ia e^{\phi + i\psi}$ ($\phi \geq 0$), one obtains $(x, y) = 2a(\cosh \phi \cos(\psi + \pi), \sinh \phi \sin(\psi + \pi))$, representing an ellipse of width $4a \cosh \phi$ and thickness $4a \sinh \phi$ [55].

The velocity field is computed by applying the conformal mapping to the complex velocity potential W of the

vortex in the ζ -plane,

$$W = -i \frac{\kappa}{2\pi} \log \zeta. \quad (5)$$

The circulation $\kappa = \frac{2\pi \hbar}{M}$ around a quantized vortex is conserved in the transformation as follows. By applying the transformation to Eq. (5) and using the formula $v \rightarrow \pm \frac{\kappa}{2\pi} \frac{1}{\sqrt{4a^2 - y^2}}$ for $|y| < 2a$ in the limit $x \rightarrow \pm 0$, the vorticity $\omega_z(x, y) = (\nabla \times \mathbf{v}_0)_z$ forms a segment singularity of width $4a$,

$$\omega_z(\mathbf{r}) = \frac{\kappa}{\pi} \frac{1}{\sqrt{4a^2 - y^2}} \delta(x) \Theta(2a - |y|). \quad (6)$$

with the step function Θ ($\Theta = 1$ for $2a \geq |y|$ and $\Theta = 0$ for $2a < |y|$). By integrating Eq. (6), it is confirmed that the circulation is conserved via the transformation; $\int dx dy \omega_z = \kappa$.

Hydrodynamic potential— To reveal the physical mechanism that stabilizes the elliptic vortex, the energy E_{vortex} of a vortex of unit length is evaluated. The vortex energy in the ζ -plane is computed conventionally by considering the contribution from the core region ($|\zeta| < \rho_{\text{core}} \equiv a e^{\phi_{\text{core}}}$) and the outer region ($|\zeta| > \rho_{\text{core}}$) separately [56]. Similarly, we consider the Joukowski mapping of the former and the latter, corresponding to an ellipse of area S_{core} and outer area S_{out} in the xy -plane, respectively.

The core region is characterized by two parameters a and $r_{\text{core}} \equiv \rho_{\text{core}} - a$ as

$$S_{\text{core}} = \pi R_+ R_- = \pi \frac{(a + r_{\text{core}})^4 - a^4}{(a + r_{\text{core}})^2}, \quad (7)$$

with $R_{\pm} = \frac{(a + r_{\text{core}})^2 \pm a^2}{a + r_{\text{core}}}$. Here, $2R_{+(-)}$ is the length of the major (minor) axis of the ellipse. For high oblateness with $\frac{a}{r_{\text{core}}} \gg 1$, we have $R_+ \approx 2a$ and $R_- \approx 2r_{\text{core}}$, and the width and thickness of the core region are in the order of $4a$ and $4r_{\text{core}}$, respectively. We have $R_+ = R_- \rightarrow r_{\text{core}}$ for the axisymmetric limit $\frac{a}{r_{\text{core}}} \rightarrow 0$.

The vortex energy is defined as the excess energy in the presence of the vortex, with respect to the bulk energy $E_{\text{bulk}} = \mathcal{U}_P(S_{\text{in}} + S_{\text{out}})$ with energy density $\mathcal{U}_P = -\frac{1}{2} \mu n_P$ of the P state. The vortex energy is then represented formally by

$$E_{\text{vortex}} = E_{\text{out}} + E_{\text{core}} - E_{\text{bulk}} = U_{\text{core}} + U_{\text{out}} \quad (8)$$

with $E_{\text{core(out)}} = \int_{S_{\text{core(out)}}} dx dy \mathcal{G}$ and $U_{\text{core(out)}} = E_{\text{core(out)}} - \mathcal{U}_P S_{\text{core(out)}}$. The potential U_{out} of the outer region is evaluated by computing the integral in E_{out} analytically with an approximation $n \approx n_P \left(1 - \frac{M}{2\mu} v_0^2\right)$, where the quantum pressure is neglected. In the approximation up to the order of $\mathcal{O}\left(\frac{M}{2\mu} v_0^2\right)$, a straightforward computation yields

$$U_{\text{out}} \approx U_{\text{hyd}} = \frac{M n_P \kappa^2}{4\pi} \ln \frac{R}{a + r_{\text{core}}}. \quad (9)$$

Here, we used the radius $R = ae^{\phi_{\text{out}}}$ of the system boundary by assuming $R \gg a$ [57].

Elastic core potential— The core potential is determined by introducing a phenomenological model, where a soliton is spanned between the spin spots. This model is justified by the fact that the phase gradient is mainly concentrated around the spin spots, consistent with the vorticity distribution (6) [see also Fig. 1(c)]; thus, the core structure between the spots is similar to that of the AF-core soliton [46]. Accordingly, we write

$$U_{\text{core}} = E_{\text{soliton}} + E_{\text{spin}} \quad (10)$$

where the soliton energy E_{soliton} is a function of the length $l_{\text{soliton}} \sim l_{\text{spot}}$ and the spin interaction E_{spin} comes from the second term of Eq. (1).

It is important to note that U_{core} depends explicitly on l_{spot} through E_{soliton} . This is because E_{spin} is determined independently from the hydrodynamic argument. The size r_{spin} and the magnitude $s_{\perp}^{\text{max}} = \max(s_y)$ of the spin spot are asymptotic to $\xi_s = \frac{\hbar}{\sqrt{Mc_2 n_P}}$ and n_P , respectively, for $\xi_q \gg \xi_s \gg \xi_n$. For $\xi_s \gg \xi_q \gtrsim \xi_n$, the core density grows as $n_{\pm 1}(0) \propto 1 - \frac{q}{qc}$ in the continuous phase transition [58], and the size r_{spin} must be bounded below the vortex core size $\lesssim \xi_q$. Therefore, the size of a spin spot is simply parameterized as

$$r_{\text{spin}}^{-1} = \xi_s^{-1} + C_{\text{spin}} \xi_q^{-1} \quad (11)$$

with a constant $C_{\text{spin}} \sim \mathcal{O}(1)$. In fact, the spin interaction, estimated by $E_{\text{spin}} = \frac{1}{2}c_2(s_y^{\text{max}})^2\pi r_{\text{spin}}^2$ agrees well with the numerical result with $C_{\text{spin}} = 0.8$ [Fig. 2 (b)] [59].

To simplify the analysis, the soliton length is defined as $l_{\text{soliton}} \equiv 4a + 4r_{\text{core}}$. The equilibrium length is then determined by $\frac{\partial}{\partial l_{\text{soliton}}} E_{\text{vortex}} = \frac{\partial}{\partial l_{\text{soliton}}} (U_{\text{hyd}} + E_{\text{soliton}}) = 0$. In the first approximation, the soliton energy E_{soliton} is expressed as $E_{\text{soliton}}^{\text{1st}} = \alpha_{\text{AF}} l_{\text{soliton}}$ with the tension coefficient $\alpha_{\text{AF}} \sim \sqrt{q\mu} n_P \xi_n$ of the AF-core soliton [46]. This approximation fails for $\xi_q \gg \xi_s$. Actually, the thickness of the elliptic core is much smaller than the thickness $\sim \xi_q$ of the AF-core soliton forming a halo structure [Fig. 1 (a)], which increases the tension effectively. To take this effect into account, we introduce a phenomenological formula

$$\frac{E_{\text{soliton}}}{\mu n_P \xi_n^2} = \sqrt{\frac{q}{\mu}} \frac{l_{\text{soliton}}}{\xi_n} \left(1 + \frac{l_{\text{soliton}}}{r_{\text{spin}}} \right). \quad (12)$$

This formula yields $l_{\text{soliton}} = \frac{r_{\text{spin}}}{4\xi_n} \left(\sqrt{1 + 8\pi \frac{\xi_q}{r_{\text{spin}}}} - 1 \right)$, and explains the scaling behavior of l_{spin} in Fig. 2(a). This means that the soliton is effectively elastic with $E_{\text{soliton}} \propto l_{\text{soliton}}^2$ for $\xi_q \gg \xi_s$ with $r_{\text{spin}} \sim \xi_s$.

Rotating solutions— Finally, the response to an external rotation is investigated as a dynamical property. The external rotation of angular frequency Ω is introduced by $G' = G - \Omega L_z$, the energy in the rotating frame [60], with

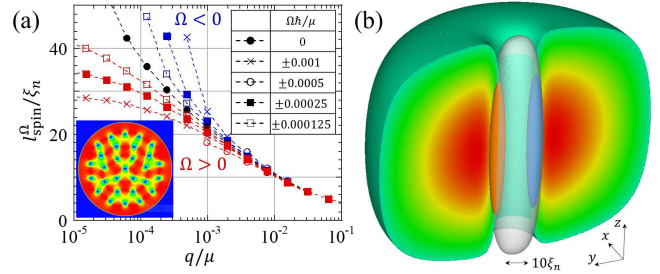


FIG. 3. (a) The q -dependence of the width l_{spin}^{Ω} of a rotating elliptic vortex with angular velocity Ω . The state with a single vortex is less stable for larger $|\Omega|$ and smaller q , leading to a lattice of elliptic vortices. The inset shows a lattice state obtained for $\Omega\hbar/\mu = 0.001$ and $q/\mu = 2^{-11}$. (b) The three dimensional solution of an elliptic vortex in a harmonic trap for $\Omega\hbar/\mu = 0.0005$. The isovolume plot shows the region $|\Psi_0|^2 c_0/\mu \leq 0.3$ for $x > 0$ and the density $|\Phi_0|^2$ in the $x = 0$ cross-section is displayed. A translucent surface along the z axis represents the isosurface of $|\Psi_{\pm 1}|^2 c_0/\mu = 0.15$, to which the two poles of the isosurfaces $s_y c_0/\mu = \pm 0.7$ are attached (red for positive and blue for negative).

the angular momentum L_z of the condensate along the rotation (z) axis. The width l_{spin}^{Ω} of an elliptic vortex decreases with Ω [Fig. 3(a)], since the angular momentum increases more as the vorticity is localized more toward the center. Owing to the boundary effect [61], the solutions of a single vortex are unstable for large $|\Omega|$ or small q/μ , leading to a lattice of elliptic vortices [inset of Fig. 3(a)].

The three-dimensional structure of an elliptic vortex is demonstrated numerically for a feasible setup in Fig. 3(b). A condensate of $N \approx 5.6 \times 10^5$ ^{23}Na atoms is trapped by a harmonic potential $V_{\text{trap}} = \frac{M}{2}(\omega_{\perp}^2 r^2 + \omega_z^2 z^2)$ with $\frac{\hbar}{\mu}(\omega_{\perp}, \omega_z) \approx (0.019, 0.024)$. The spin spots appear as two poles (red and blue) along the $m = \pm 1$ component (translucent pole) in the vortex core of the $m = 0$ component [62].

Summary and discussion— The oblateness of the elliptic vortex increases with ξ_q and becomes large, notably when the spin interaction is maximized for $\xi_q \gg \xi_s \gg \xi_n$. The elliptic core is sustained by the repulsive hydrodynamic and attractive elastic potentials, which are observed as two spin spots (poles) with *in situ* magnetization imaging [21].

The analysis implies that the wall-HQV composites [30, 31] can survive as elliptic vortices after the quenched phase transition, although they were assumed to be marginally unstable for $q \rightarrow 0$, owing to the snake instability. The logics and analyses here can be applied in a similar way to the double-core vortex or the KLS-wall-HQV composite in superfluid $^3\text{He-B}$, while different forms of the hydrodynamic potential and soliton tension were introduced [63]. It should be mentioned that similar objects are observed as the spin-mass vortex attached

by a planar soliton in superfluid ^3He [64, 65] and has been investigated theoretically as the vortex molecules in Rabi-coupled binary BECs [66–74]. Further investigations on the dynamics and interactions of the wall-HQV composites will shed light on unexplored phenomena of symmetry breaking phase transitions.

H.T. thanks Yong-il Shin for discussion and critical reading of the manuscript. This work is supported by JSPS KAKENHI Grant Numbers JP17K05549, JP18KK0391, JP20H01842, and in part by the OCU "Think globally, act locally" Research Grant for Young Scientists 2019 and 2020 through the hometown donation fund of Osaka City.

* takeuchi@osaka-cu.ac.jp; <http://hiromitsu-takeuchi.appspot.com>

- [1] Dieter Vollhardt and Peter Wolfle. *The superfluid phases of helium 3*. Courier Corporation, 2013.
- [2] Kenichi Kasamatsu, Makoto Tsubota, and Masahito Ueda. Vortices in multicomponent Bose–Einstein condensates. *International Journal of Modern Physics B*, 19(11):1835–1904, 2005.
- [3] Yuki Kawaguchi and Masahito Ueda. Spinor Bose–Einstein Condensates. *Physics Reports*, 520(5):253–381, 2012.
- [4] S. Chandrasekhar. *Liquid Crystals*. Cambridge University Press, 2 edition, 1992.
- [5] The term "nematic-spin" or "spin-nematic" has been also used in the literatures of different condensed matter systems, e.g., the spin-nematic phase in antiferromagnets [6] and the nematic-spin fluid in BaFe_2As_2 [7].
- [6] Hirokazu Tsunetsugu and Mitsuhiro Arikawa. Spin nematic phase in $s=1$ triangular antiferromagnets. *Journal of the Physical Society of Japan*, 75(8):083701, 2006.
- [7] L. W. Harriger, H. Q. Luo, M. S. Liu, C. Frost, J. P. Hu, M. R. Norman, and Pengcheng Dai. Nematic spin fluid in the tetragonal phase of BaFe_2As_2 . *Phys. Rev. B*, 84:054544, Aug 2011.
- [8] N. D. Mermin. The topological theory of defects in ordered media. *Rev. Mod. Phys.*, 51:591–648, Jul 1979.
- [9] PB Sunil Kumar and GS Ranganath. On certain liquid crystal defects in a magnetic field. *Molecular Crystals and Liquid Crystals*, 177(1):131–144, 1989.
- [10] Grigory E Volovik. *Exotic properties of superfluid ^3He* , volume 1. World Scientific, 1992.
- [11] V. P. Mineyev and G. E. Volovik. Planar and linear solitons in superfluid ^3He . *Phys. Rev. B*, 18:3197–3203, Oct 1978.
- [12] Fei Zhou. Spin Correlation and Discrete Symmetry in Spinor Bose-Einstein Condensates. *Phys. Rev. Lett.*, 87:080401, Aug 2001.
- [13] Fei Zhou. Quantum spin nematic states in Bose–Einstein condensates. *International Journal of Modern Physics B*, 17(14):2643–2698, 2003.
- [14] J. Ruostekoski and J. R. Anglin. Monopole Core Instability and Alice Rings in Spinor Bose-Einstein Condensates. *Phys. Rev. Lett.*, 91:190402, Nov 2003.
- [15] N. D. Mermin. *Surface Singularities and Superflow in $^3\text{He-A}$* , pages 3–22. Springer US, Boston, MA, 1977.
- [16] GE Volovik. Defects at interface between A and B phases of superfluid ^3He . *JETP Lett*, 51(8), 1990.
- [17] T Sh Misirpashaev. The topological classification of defects at a phase interface. *Soviet physics, JETP*, 72(6):973–982, 1991.
- [18] Hiromitsu Takeuchi and Makoto Tsubota. Boojums in rotating two-component Bose-Einstein condensates. *Journal of the Physical Society of Japan*, 75(6):063601, 2006.
- [19] U. Leonhardt and G.E. Volovik. How to create Alice string (half quantum vortex) in a vector Bose-Einstein condensate. *Pisma Zh. Eksp. Teor. Fiz.*, 72:66–70, 2000.
- [20] M. R. Matthews, B. P. Anderson, P. C. Haljan, D. S. Hall, C. E. Wieman, and E. A. Cornell. Vortices in a Bose-Einstein Condensate. *Phys. Rev. Lett.*, 83:2498–2501, Sep 1999.
- [21] Sang Won Seo, Seji Kang, Woo Jin Kwon, and Yong-il Shin. Half-Quantum Vortices in an Antiferromagnetic Spinor Bose-Einstein Condensate. *Phys. Rev. Lett.*, 115:015301, Jul 2015.
- [22] S. Autti, V. V. Dmitriev, J. T. Mäkinen, A. A. Soldatov, G. E. Volovik, A. N. Yudin, V. V. Zavjalov, and V. B. Eltsov. Observation of Half-Quantum Vortices in Topological Superfluid ^3He . *Phys. Rev. Lett.*, 117:255301, Dec 2016.
- [23] Y. Kondo, J. S. Korhonen, M. Krusius, V. V. Dmitriev, Y. M. Mukharsky, E. B. Sonin, and G. E. Volovik. Direct observation of the nonaxisymmetric vortex in superfluid $^3\text{He-B}$. *Phys. Rev. Lett.*, 67:81–84, Jul 1991.
- [24] JT Mäkinen, VV Dmitriev, Jaakko Nissinen, Juho Rysti, GE Volovik, AN Yudin, Kuang Zhang, and VB Eltsov. Half-quantum vortices and walls bounded by strings in the polar-distorted phases of topological superfluid ^3He . *Nature communications*, 10(1):1–8, 2019.
- [25] G. E. Volovik and K. Zhang. String monopoles, string walls, vortex skyrmions, and nexus objects in the polar distorted B phase of ^3He . *Phys. Rev. Research*, 2:023263, Jun 2020.
- [26] K Zhang. One dimensional nexus objects, network of Kibble-Lazarides-Shafi string walls, and their spin dynamic response in polar distorted B-phase of ^3He . *arXiv preprint arXiv:2008.09286*, 2020.
- [27] T. W. B. Kibble, G. Lazarides, and Q. Shafi. Walls bounded by strings. *Phys. Rev. D*, 26:435–439, Jul 1982.
- [28] T.W.B. Kibble, G. Lazarides, and Q. Shafi. Strings in $so(10)$. *Physics Letters B*, 113(3):237 – 239, 1982.
- [29] T.W. B. Kibble. *Topological Defects and the Non-Equilibrium Dynamics of Symmetry Breaking Phase Transitions*, volume 549. Springer Netherlands, 2000.
- [30] Seji Kang, Sang Won Seo, Hiromitsu Takeuchi, and Y. Shin. Observation of Wall-Vortex Composite Defects in a Spinor Bose-Einstein Condensate. *Phys. Rev. Lett.*, 122:095301, Mar 2019.
- [31] Seji Kang, Deokhwa Hong, Joon Hyun Kim, and Y. Shin. Crossover from weak to strong quench in a spinor Bose-Einstein condensate. *Phys. Rev. A*, 101:023613, Feb 2020.
- [32] Takafumi Kita. Unconventional vortices and phase transitions in rapidly rotating superfluid ^3He . *Phys. Rev. B*, 66:224515, Dec 2002.
- [33] M. A. Silaev, E. V. Thuneberg, and M. Fogelström. Lifshitz Transition in the Double-Core Vortex in $^3\text{He-B}$. *Phys. Rev. Lett.*, 115:235301, Dec 2015.
- [34] Kenichi Kasamatsu, Ryota Mizuno, Tetsuo Ohmi, and Mikio Nakahara. Effects of a magnetic field on vortex states in superfluid $^3\text{He-B}$. *Phys. Rev. B*, 99:104513,

- Mar 2019.
- [35] Masaki Tange and Ryusuke Ikeda. Half-quantum vortex pair in the polar-distorted B phase of superfluid ^3He in aerogels. *Phys. Rev. B*, 101:094512, Mar 2020.
- [36] Robert C. Regan, J. J. Wiman, and J. A. Sauls. Vortex phase diagram of rotating superfluid ^3He -B. *Phys. Rev. B*, 101:024517, Jan 2020.
- [37] Subroto Mukerjee, Cenke Xu, and J. E. Moore. Topological Defects and the Superfluid Transition of the $s = 1$ Spinor Condensate in Two Dimensions. *Phys. Rev. Lett.*, 97:120406, Sep 2006.
- [38] A. J. A. James and A. Lamacraft. Phase Diagram of Two-Dimensional Polar Condensates in a Magnetic Field. *Phys. Rev. Lett.*, 106:140402, Apr 2011.
- [39] Michikazu Kobayashi. Berezinskii-Kosterlitz-Thouless Transition of Spin-1 Spinor Bose Gases in the Presence of the Quadratic Zeeman Effect. *Journal of the Physical Society of Japan*, 88(9):094001, 2019.
- [40] Christopher J Pethick and Henrik Smith. *Bose-Einstein condensation in dilute gases*. Cambridge university press, 2008.
- [41] Tetsuo Ohmi and Kazushige Machida. Bose-Einstein condensation with internal degrees of freedom in alkali atom gases. *Journal of the Physical Society of Japan*, 67(6):1822–1825, 1998.
- [42] The vortex solution is obtained by minimizing the energy functional with the steepest descent method [43]. The condensate is trapped by a cylindrical box potential. The system size is enough large to neglect the boundary effect. The boundary effect becomes significant when the distance l_{spin} between the spin spots becomes $\gtrsim R/2$ with the system size $R = 410\xi_n$. The details of the numerical method and the cross-section profile for different values of q/μ are demonstrated in the supplemental material. For the dependence of l_{spin} on q/μ , see also Fig. 2(a).
- [43] Haskell B Curry. The method of steepest descent for non-linear minimization problems. *Quarterly of Applied Mathematics*, 2(3):258–261, 1944.
- [44] Neglecting the spin interaction with $\frac{c_1}{c_0} = 0.016 \ll 1$, the critical value is determined $q_C/\mu \approx 0.25$ by regarding $\Phi_{\pm 1}$ as a single particle wave function bounded by the vortex core of Φ_0 . A similar problem is solved for the nematic-spin vortex in the AF phase [45].
- [45] Andrew P. C. Underwood, D. Baillie, P. Blair Blakie, and H. Takeuchi. Properties of a nematic spin vortex in an antiferromagnetic spin-1 Bose-Einstein condensate. *Phys. Rev. A*, 102:023326, Aug 2020.
- [46] I Liu, Shih-Chuan Gou, Hiromitsu Takeuchi, et al. Phase Diagram of Solitons in the Polar Phase of a Spin-1 Bose-Einstein Condensate. *Phys. Rev. Research, in press (2020)*; *arXiv preprint arXiv:2002.06088*, 2020.
- [47] According to the rotational symmetry about the z axis of the energy functional in the spin space, the orientation of the transverse magnetization in the xy -plane can be taken to be arbitrary depending on the relative phase between Φ_0 and $\Phi_{\pm 1}$. Similarly, the direction of the elliptic structure depends on the phases.
- [48] To avoid the singularity of Θ_0 for $d_z = 0$, Φ_0 is replaced by $\arg \Phi_{x(y)}$ with $d_{x(y)} > 0$ and $e_{x(y)} = 0$.
- [49] A similar rule has been introduced in Ref. [50], where the quadratic Zeeman effect is absent.
- [50] Tomoya Isoshima, Kazushige Machida, and Tetsuo Ohmi. Quantum Vortex in a Spinor Bose-Einstein Condensate. *Journal of the Physical Society of Japan*, 70(6):1604–1610, 2001.
- [51] The z component of the spin density is written as $s_z = |\Phi_1|^2 - |\Phi_{-1}|^2$.
- [52] The elliptic velocity field also recalls us the Kirchhoff elliptic vortex [53]. However, the dynamical property is different in a sense that the elliptic vortex in our system is stationary while the Kirchhoff vortex is rotating in general (see e.g., [54]). The method of the Joukowski mapping justifies the existence of a stationary solution of an elliptic vortex.
- [53] Gustav Kirchhoff. *Vorlesungen über mathematische physik: mechanik*, volume 1. BG Teubner, 1876.
- [54] TB Mitchell and LF Rossi. The evolution of Kirchhoff elliptic vortices. *Physics of Fluids*, 20(5):054103, 2008.
- [55] The phase $\arg(ia)$ determines the direction of the ellipse. The ellipse is along the x axis when ia is replaced by a . The phase is set so as to make the ellipse along the y axis, which is consistent with Fig. 1.
- [56] Russell J Donnelly. *Quantized vortices in helium II*, volume 2. Cambridge University Press, 1991.
- [57] The details of the derivation of the hydrodynamic potential is described in the supplemental material.
- [58] A similar behavior was found in the continuous phase transition of the core state of soliton and vortex in spinor BECs [45, 46].
- [59] The details of the computation of the spin interaction is described in the supplemental material while the computation is not directly relevant to the validity of the main results.
- [60] Lev Davidovich Landau, Evgenij Mihajlovič Lifšic, Evgenii Mikhailovich Lifshitz, and LP Pitaevskii. *Statistical physics: theory of the condensed state*, volume 9. Butterworth-Heinemann, 1980.
- [61] The boundary effect is caused by the nucleation of vortices at the system boundary, which occurs if $|\Omega|$ exceeds a critical value.
- [62] In the local density approximation, the effective chemical potential is written as $\mu' = \mu - V_{\text{trap}}$. According to Fig. 2(b), the spin density decreases with q/μ' . This is why the spin poles become thinner as they are away from the trap center. The vortex core size becomes thicker as the local healing length $\frac{\hbar}{\sqrt{M\mu'}}$ becomes larger for large $|z|$.
- [63] G Volovik. Half-quantum vortices in superfluid ^3He -B. *JETP Lett*, 52(6), 1990.
- [64] Y. Kondo, J. S. Korhonen, M. Krusius, V. V. Dmitriev, E. V. Thuneberg, and G. E. Volovik. Combined spin-mass vortex with soliton tail in superfluid ^3He -B. *Phys. Rev. Lett.*, 68:3331–3334, Jun 1992.
- [65] Olli V. Lounasmaa and Erkki Thuneberg. Vortices in rotating superfluid ^3He . *Proceedings of the National Academy of Sciences*, 96(14):7760–7767, 1999.
- [66] D. T. Son and M. A. Stephanov. Domain walls of relative phase in two-component Bose-Einstein condensates. *Phys. Rev. A*, 65:063621, Jun 2002.
- [67] Kenichi Kasamatsu, Makoto Tsubota, and Masahito Ueda. Vortex Molecules in Coherently Coupled Two-Component Bose-Einstein Condensates. *Phys. Rev. Lett.*, 93:250406, Dec 2004.
- [68] Mattia Cipriani and Muneto Nitta. Crossover between Integer and Fractional Vortex Lattices in Coherently Coupled Two-Component Bose-Einstein Condensates. *Phys. Rev. Lett.*, 111:170401, Oct 2013.

- [69] Marek Tylutki, Lev P. Pitaevskii, Alessio Recati, and Sandro Stringari. Confinement and precession of vortex pairs in coherently coupled Bose-Einstein condensates. *Phys. Rev. A*, 93:043623, Apr 2016.
- [70] Luca Calderaro, Alexander L. Fetter, Pietro Massignan, and Peter Wittek. Vortex dynamics in coherently coupled Bose-Einstein condensates. *Phys. Rev. A*, 95:023605, Feb 2017.
- [71] Minoru Eto and Muneto Nitta. Confinement of half-quantized vortices in coherently coupled Bose-Einstein condensates: Simulating quark confinement in a QCD-like theory. *Phys. Rev. A*, 97:023613, Feb 2018.
- [72] A. Gallemí, L. P. Pitaevskii, S. Stringari, and A. Recati. Decay of the relative phase domain wall into confined vortex pairs: The case of a coherently coupled bosonic mixture. *Phys. Rev. A*, 100:023607, Aug 2019.
- [73] Kousuke Ihara and Kenichi Kasamatsu. Transverse instability and disintegration of a domain wall of a relative phase in coherently coupled two-component Bose-Einstein condensates. *Phys. Rev. A*, 100:013630, Jul 2019.
- [74] Michikazu Kobayashi, Minoru Eto, and Muneto Nitta. Berezinskii-Kosterlitz-Thouless Transition of Two-Component Bose Mixtures with Intercomponent Josephson Coupling. *Phys. Rev. Lett.*, 123:075303, Aug 2019.

SUPPLEMENTAL MATERIAL

Method of the numerical simulation

Here, we describe the method of numerical simulation used in this work. The numerical solutions is obtained by minimizing the energy functional

$$G'' = \int_{-R_1}^{R_1} dx \int_{-R_2}^{R_2} dy \int_{-R_3}^{R_3} dz d^3x (\mathcal{G} + V_{\text{trap}} n - \Omega l_z)$$

with the trapping potential V_{trap} and $l_z = \hbar \sum_m \Re[\Phi_m x \partial_y \Phi_m - y \partial_x \Phi_m]$. The space coordinates $(x, y, z) = (x_1, x_2, x_3)$ are discretized as $x_i(n_i) = -R_i + \Delta x n_i$ with $n_i = 0, 1, 2, \dots, N_i$ with $x_i(N_i) = R_i$. The spatial derivatives of Φ_m are computed with finite difference approximation; e.g., $\partial_x \Phi_m$ and $\partial_x^2 \Phi_m$ are computed by the central difference of the first and second order, respectively.

All solutions were obtained by minimizing the energy functional very carefully. The steepest descent method is performed by solving the imaginary time evolution $\frac{\partial \Phi_m}{\partial \tau} = -\frac{\delta G''}{\delta \Phi_m}$. The imaginary time τ is discretized as $\tau = \Delta \tau n_\tau$ with $n_\tau = 0, 1, 2, \dots$. The time evolution is written as $\Phi_m(n_\tau + 1) = \Phi_m(n_\tau) - \Delta \tau \frac{\delta G''}{\delta \Phi_m}(n_\tau)$. The time evolution is computed until the difference $G''(n_\tau) - G''(n_\tau - 1000)$ becomes non-negative within the double precise by using Intel[®] Fortran Compiler.

The solutions in a uniform system is approximately obtained in a cylindrical box potential $V_{\text{trap}} = V_0[\tanh(r - R) + 1]$ with $V_0/\mu = 20$, $R = 0.95R_\perp$, and $R_1 = R_2 = R_\perp$. Here, we solve two-dimensional equations by assuming that the wave functions are homogeneous along the z axis and thus independent of z . The trap depth V_0 is taken to be so large that the order parameter damps quickly outside the cylinder and almost vanish nearby the system boundary. For the non-rotating case of $\Omega = 0$ (the results of Figs. 1 and 2), the numerical simulation was done with $2R_\perp = 1024.5\xi_n$ with $N_1 = N_2 = 2048$, $\Delta x = 0.5\xi_n$, and $\Delta \tau = 0.0025$. It was confirmed that our results do not change essentially for $\Delta x = 0.3\xi_n$ and $\Delta x = 0.4\xi_n$ except for the finite-size effect, which is of no interest to our main subject. The finite-size effect becomes important only for $\frac{q}{\mu} \leq 2^{-19} \approx 1.9 \times 10^{-6}$ for $\Delta = 0.5\xi_n$. For very small values of $\frac{q}{\mu}$ the width of the elliptic vortex become on the order of or larger than the system size and we could not obtain the vortex state.

The vortex solutions were obtained for $q/\mu = 2^{-n_q}$ ($n_q = 0, 1, 2, \dots$) as shown in Fig. A1. The vortex has the normal core with $\Phi_{\pm 1} = 0$ for $n_q < 3$ (not shown). The protocol of the numerical simulation is as follows. First, the solution for $n_q = 3$ is obtained. Then, the initial state of the time evolution is set as $\Phi_0 = f_0(r)e^{i\varphi}$ and $\Phi_{\pm 1} = f_{\pm 1}$ with $f_0(r) = \sqrt{\max(0, \mu - V_{\text{trap}} - \frac{\hbar^2}{2Mr^2})}$ and $f_{\pm 1}(r) = \pm \sqrt{\frac{n_q}{2}} e^{-r^2/\xi_n^2}$. The vortex can be stabilized in the center region even for the non-rotating case

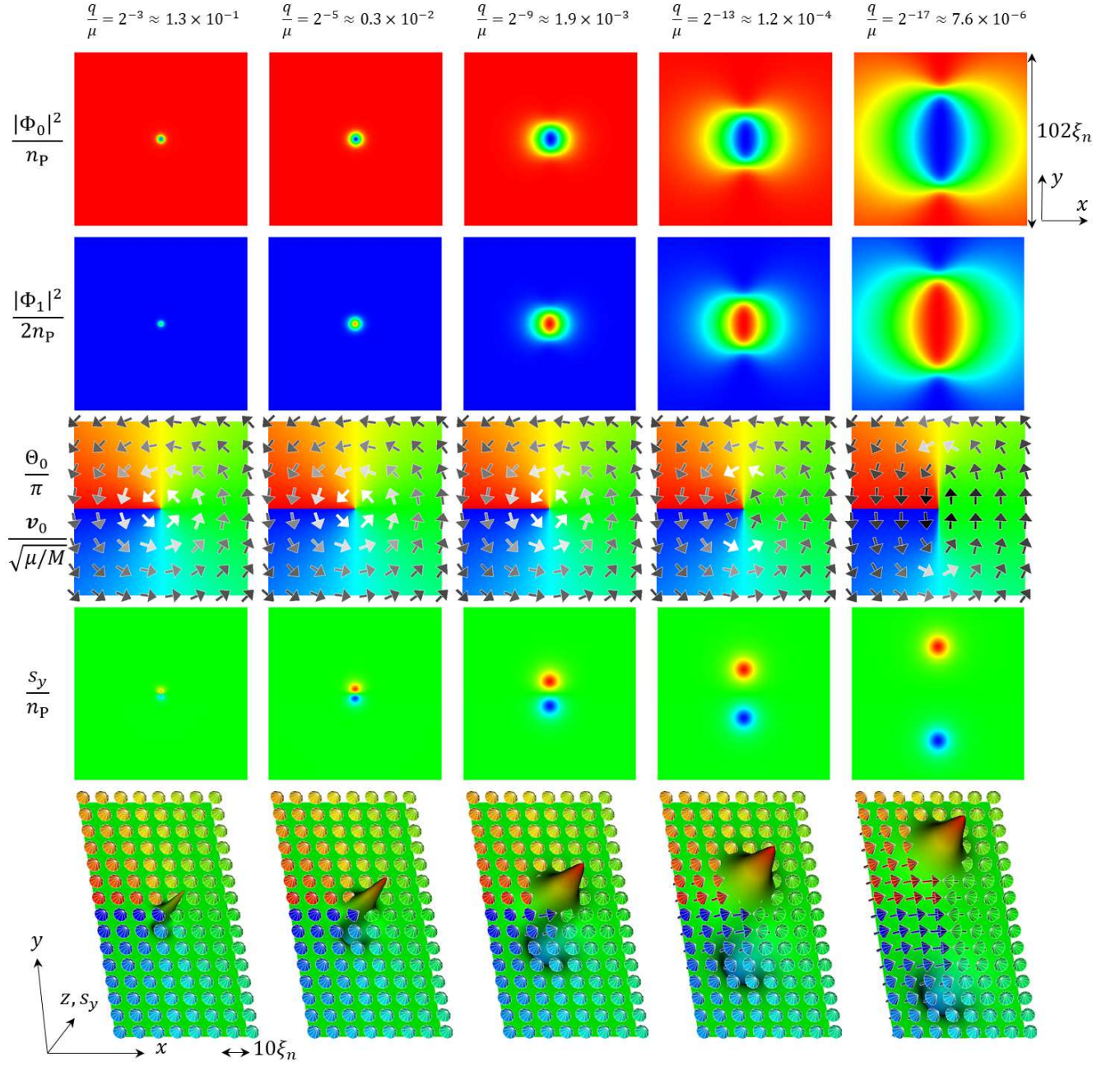


FIG. A1. The cross-sectional profiles of elliptic vortices and the three dimensional texture of pseudo-director field $\mathbf{d}/|\mathbf{d}|$ for $q = 2^{-n_q}$ ($n_q = 3, 5, 9, 13, 17$). The method of plot is the same as that of Fig. 1 in the main text. The angle of view is changed from that in Fig. 1 in the three dimensional plots in the bottom.

of $\Omega = 0$ since the spatial gradient of V_{trap} is negligibly small there. The solution for $n_q + 1$ is obtained by using the solution of n_q as the initial state.

The rotating case of Fig. 3 (a) is obtained with $2R_{\perp} = 410\xi_n$ with $N_1 = N_2 = 1048$ and $\Delta = 0.4\xi_n$. The protocol is the same as the non-rotating case. For the three dimensional simulation in the harmonic trap of Fig. 3 (b), the system size is $2R_{\perp} = 192.5\xi_n$ and $2R_z = 128.5\xi_n$ with $N_1 = N_2 = 384$, $N_3 = 256$ and $\Delta = 0.5\xi_n$.

Computation of the hydrodynamic potential

The velocity field $\mathbf{v} = (u, v)^T$ in a two dimensional potential flow is represented as $u = \partial_y \Psi = \partial_x \Phi$ and $v = -\partial_x \Psi = \partial_y \Phi$ with the Stream function Ψ and the velocity potential Φ . The complex velocity potential $W = \Phi + i\Psi$ of a point vortex with a circulation Γ in the complex plane (x, y) is written as $W = -i\frac{\Gamma}{2\pi} \log z$. The Joukowski transformation $z = \zeta + \frac{a^2}{\zeta}$ with $\zeta = ae^{\phi+\psi}$

reads $x = 2a \cosh \phi \cos \psi$ and $y = 2a \sinh \phi \sin \psi$. This transformation corresponding to an ellipse of major radius $2a \cosh \phi$ and minor radius $2a \sinh \phi$ ($\phi \geq 0$) in the xy -plane. The ellipse reduces a segment of length $4a$ along the x axis for $\phi = 0$. The segment is along the y axis if a is replaced by ia in the formula of ζ . We used the formula $\zeta = ae^{\phi+i\psi}$ in the following computation without loss of generality.

In a quantized vortex in a scalar superfluid, the velocity field diverges at the center of the vortex core, where the order parameter amplitude vanishes at the core. The density increases to the bulk value far from the core. The region within a circle of a radius ξ_n with small density around the center is called the core region. To evaluate the energy of a quantized vortex per unit length, the contributions from the core region ($r < \xi_n$) and its outer region ($r > \xi_n$) is computed separately. Similarly, for the elliptic vortex, there exists the core region of an elliptic form around the band-shaped singularity and the energy is computed separately.

To compute the energy analytically, we neglect the so-called quantum pressure term in the Thomas-Fermi (TF) approximation [40]. Then, the density far from the vortex core can be written as

$$n \approx n_{\text{TF}} = n_{\text{bulk}} \left(1 - \frac{M}{2\mu} \mathbf{v}^2 \right)$$

with $n_{\text{bulk}} = n_{\text{P}}$ is the bulk density. In this approximation, one obtains the contribution to the energy functional G from the outer region of area S_{out} up to the order of $\mathcal{O} \left(\frac{M}{2\mu} \mathbf{v}^2 \right)$

$$\begin{aligned} E_{\text{out}} &= \int_{S_{\text{out}}} d^2x \mathcal{G} \\ &\approx \int_{S_{\text{out}}} d^2x \left[\frac{Mn_{\text{TF}}}{2} \mathbf{v}^2 + \mathcal{U}(n_{\text{TF}}) \right] \\ &= \int_{S_{\text{out}}} d^2x \left[\frac{Mn_{\text{P}}}{2} \mathbf{v}^2 + \mathcal{U}_{\text{P}} \right]. \end{aligned} \quad (\text{A1})$$

Here, $\mathcal{U}(n_{\text{TF}})$ is the energy density \mathcal{U} evaluated in the TF approximation, and it reduces to, for the bulk in the P state,

$$\mathcal{U}_{\text{bulk}} = \mathcal{U}_{\text{P}} = -\frac{\mu^2}{2c_0}.$$

A state, different from the P state, appears in the core region where the $m = 0$ component vanishes. The contribution from the core region is written as

$$E_{\text{core}} = \mathcal{U}_{\text{core}} S_{\text{core}}$$

with the energy density $\mathcal{U}_{\text{core}}$ and the area S_{core} of the core region.

The vortex energy E_{vortex} is defined as an excess energy in the presence of the vortex, the difference between the total energy with a vortex and the energy

$E_{\text{bulk}} = \mathcal{U}_{\text{bulk}}(S_{\text{core}} + S_{\text{out}})$ in the absence of it;

$$\begin{aligned} E_{\text{vortex}} &= E_{\text{out}} + E_{\text{core}} - E_{\text{bulk}} \\ &= U_{\text{out}} + U_{\text{core}} \end{aligned} \quad (\text{A2})$$

with $U_{\text{core(out)}} = E_{\text{core(out)}} - \mathcal{U}_{\text{P}} S_{\text{core(out)}}$. The potentials of the outer and core regions are rewritten as

$$\begin{aligned} U_{\text{out}} &= \frac{Mn_{\text{bulk}}}{2} \int_{S_{\text{out}}} d^2x \mathbf{v}^2 \\ U_{\text{core}} &= \delta \mu n_{\text{bulk}} S_{\text{core}} \end{aligned} \quad (\text{A3})$$

with $\delta = \frac{\mathcal{U}_{\text{core}}}{\mu n_{\text{bulk}}} + \frac{1}{2}$.

The potential U_{out} , which is reduced to the hydrodynamic potential U_{hyd} as shown later, is evaluated by computing the integral

$$\begin{aligned} I &= \int_{S_{\text{out}}} dx dy \mathbf{v}^2 \\ &= \left(\frac{\Gamma}{2\pi} \right)^2 \int_{S_{\text{out}}} dx dy \left| \frac{1}{\sqrt{z^2 - 4a^2}} \right|^2 \\ &= \left(\frac{\Gamma}{2\pi} \right)^2 \int_{S_{\text{out}}} dx dy \frac{1}{\sqrt{(x^2 - y^2 - 4a^2)^2 + 4x^2 y^2}}. \end{aligned}$$

Here, we used

$$|u| = \frac{\Gamma}{2\pi} \left| \Im \left[\frac{\partial_x \zeta}{\zeta} \right] \right| = \frac{\Gamma}{2\pi} \left| \Im \left[\frac{1}{\sqrt{z^2 - 4a^2}} \right] \right|$$

and

$$|v| = \frac{\Gamma}{2\pi} \left| \Im \left[\frac{\partial_y \zeta}{\zeta} \right] \right| = \pm \frac{\Gamma}{2\pi} \left| \Re \left[\frac{1}{\sqrt{z^2 - 4a^2}} \right] \right|.$$

According to the transformation (for the ellipse along the x axis)

$$(x, y) = (2a \cosh \phi \cos \psi, 2a \sinh \phi \sin \psi)$$

we have the determinant of the Jacobian matrix

$$\left| \frac{\partial(x, y)}{\partial(\phi, \psi)} \right| = 2a^2 (\cosh 2\phi - \cos 2\psi).$$

The integral I is computed as

$$\begin{aligned} I &= \left(\frac{\Gamma}{2\pi} \right)^2 \int_{\phi_{\text{core}}}^{\phi_R} d\phi \int_{-\pi}^{\pi} d\psi \frac{1}{2a^2 \sqrt{(\cosh 2\phi - \cos 2\psi)^2}} \left| \frac{\partial(x, y)}{\partial(\phi, \psi)} \right| \\ &= \frac{\Gamma^2}{2\pi} \int_{\phi_{\text{core}}}^{\phi_R} d\phi \\ &= \frac{\Gamma^2}{2\pi} (\phi_R - \phi_{\text{core}}) \\ &= \frac{\Gamma^2}{2\pi} \ln \frac{\rho_R}{\rho_{\text{core}}} \end{aligned}$$

with the radius of the system boundary in the ζ -plane

$$\rho_R = ae^{\phi_R} \text{ or } \phi_R = \ln \frac{\rho_R}{a}$$

and the cutoff radius for the core region

$$\rho_{\text{core}} = ae^{\phi_{\text{core}}} \text{ or } \phi_{\text{core}} = \ln \frac{\rho_{\text{core}}}{a} \quad (\rho_{\text{core}} > a).$$

The system boundary and the cutoff circle in the ζ -plane are mapped into ellipses in the xy -plane. The major and minor radiuses are written as

$$\begin{aligned} A_{R,\text{core}} &= 2a \cosh \phi_{R,\text{core}} = \frac{\rho_{R,\text{core}}^2 + a^2}{\rho_{R,\text{core}}} \\ B_{R,\text{core}} &= 2a \sinh \phi_{R,\text{core}} = \frac{\rho_{R,\text{core}}^2 - a^2}{\rho_{R,\text{core}}} \end{aligned} \quad (\text{A4})$$

and they satisfy the relation

$$A_{R,\text{core}} + B_{R,\text{core}} = 2\rho_{R,\text{core}}.$$

In the limit $\frac{\rho_R}{a} \rightarrow \infty$, we have

$$A_R = B_R \rightarrow \rho_R = R$$

with the radius R of the system boundary in the xy -plane.

The size of the core region is parameterized by two parameters, a and

$$r_{\text{core}} \equiv \rho_{\text{core}} - a.$$

Then, we have

$$U_{\text{out}} \approx U_{\text{hyd}} = \frac{Mn_{\text{P}}}{2} \frac{\Gamma^2}{2\pi} \ln \frac{R}{a + r_{\text{core}}}.$$

The area S_{core} of the core region is represented as

$$S_{\text{core}} = \pi A_{\text{core}} B_{\text{core}} = \pi \frac{(a + r_{\text{core}})^4 - a^4}{(a + r_{\text{core}})^2}$$

The oblateness f of the core region is defined as

$$f = 1 - \frac{B_{\text{core}}}{A_{\text{core}}} = \frac{2}{1 + (1 + r_{\text{core}}/a)^2}.$$

For $\frac{r_{\text{core}}}{a} \ll 1$, asymptotic to the limit of the maximum oblateness ($f = 1$), we have

$$A_{\text{core}} \approx 2a, \quad B_{\text{core}} \approx 2r_{\text{core}}$$

and for $\frac{r_{\text{core}}}{a} \gg 1$, asymptotic to the limit of the minimum oblateness ($f = 0$),

$$A_{\text{core}} = B_{\text{core}} \approx r_{\text{core}}.$$

The former limit corresponds to a vortex with a band-shaped core region in three dimensions, called a vortex band. The latter corresponds to a conventional vortex filament with cylindrical core region.

Computation of the spin interaction

The BA state, emerging around the edge of the elliptic vortex, is collateral in the existence of the AF state in the vortex center. Therefore, the magnetization can be associated with the density at the origin $n_{\text{core}} = n(\mathbf{r} = 0)$. According to the mean-field approach in the previous studies [45, 46], a continuous phase transition occurs at a critical point ($q = q_{\text{C}}$) in the core of a topological defect. This approach is also well applicable to our case. We obtain similar behaviors $n_{\text{core}} \propto 1 - \frac{q}{q_{\text{C}}}$ and $s_y^{\text{max}} = \max s_y \propto \sqrt{1 - \frac{q}{q_{\text{C}}}}$. Since the density is asymptotic to n_{AF} far from the critical point for $q \ll q_{\text{C}}$, a quantitative estimation is obtained by

$$n_{\text{core}} \sim n_{\text{AF}} \left(1 - \frac{q}{q_{\text{C}}}\right),$$

which is quantitatively agreed with the numerical result [Fig. 2(a)].

The magnetization is well described with this approach too. The magnetization happens around the two spots with $\arg \Phi_0 = \pm\pi$ along the y -axis. Then the local spin density is written as $F_y \sim \pm 2\sqrt{2n_1}|\Phi_0|^2$ with $\Phi_{+1} = -\Phi_{-1} = \sqrt{n_1} \propto \sqrt{n_{\text{core}}}$. The density is almost constant $n \approx n_{\text{P}}$ everywhere for small q and then the maximum value is estimated by the relation between the arithmetic and geometric means with $2n_1 = \frac{n}{2} \approx \frac{n_{\text{core}}}{2}$ and $|\Phi_0|^2 = \frac{n}{2} \approx \frac{n_{\text{P}}}{2}$ as

$$s_y^{\text{max}} \sim \frac{\sqrt{n_{\text{core}}n_{\text{P}}}}{1 + \frac{c_2}{c_0}},$$

where the factor in the denominator comes from the spin interaction in the presence of spin density.

The size r_{spin} of the magnetic spot around the edges grows with the size of the AF-core, $\sim \xi_q$. The spin interaction becomes more important as the magnetic spot grows and the spot size finally reaches the spin healing length, estimated as

$$\xi_s = \frac{\hbar}{\sqrt{M\sigma}}.$$

with $\sigma = c_2 n_{\text{P}}$. This crossover behavior of the spot size is described by a simple formula

$$r_{\text{spin}} = \frac{1}{\xi_s^{-1} + C_{\text{spin}} \xi_q^{-1}},$$

with a constant $C_{\text{spin}} \sim \mathcal{O}(1)$. Finally, the spin interaction energy is evaluated as

$$E_{\text{spin}} \sim \frac{1}{2} c_2 (s_y^{\text{max}})^2 \pi r_{\text{spin}}^2 \sim \frac{\pi}{2} \frac{c_2}{c_0} \frac{n_{\text{core}}}{n_{\text{P}}} \left(\frac{r_{\text{spin}}}{\xi_n}\right)^2 \mu n_{\text{P}} \xi_n^2.$$

This formula is well-consistent with the numerical result with $C_{\text{spin}} = 0.8$.